

OSLO SYMPOSIUM  
12-82 32 AE

MEASUREMENTS OF THE FLOW  
IN A RELATIVELY LARGE BUBBLE PLUME

by

Jerome H. Milgram

1. Introduction

Bubble plumes occur above blowouts of subsea gas-containing hydrocarbon wells and it is the desire to understand the hydrodynamics of subsea blowouts that has stimulated the most recent studies of bubble plumes. In order to increase the range of available data, plume vertical velocity measurements were made at a water depth and at gas flow rates that are intermediate between laboratory scale and well blowout scale.

These data have been combined with other available, smaller scale, data by the author to determine how the entrainment coefficient and the fraction of the momentum flux carried by the turbulence depend upon local plume properties. The results of that study will be published in the future. Here the results of the intermediate scale experiments, including implied values for the entrainment coefficient and the fraction of the momentum flux carried by the turbulence, are presented.

The method used to determine the entrainment coefficients and fractions of the momentum flux carried by the turbulence is the combination of measured data with an integral plume theory. Such an integral theory requires an initial specification for the general forms of the radial distributions of velocity and density defect. These forms are chosen to agree well with experimental findings. Gaussian forms are most commonly used and they will be used here. They are:

$$u(r,z) = U(z)e^{-r^2/b^2} \quad (1.1)$$

$$\rho_w - \rho_p(r,z) = S(z)e^{-r^2/(\lambda^2 b^2)} \quad (1.2)$$

where:  $u$  is the vertical velocity of the liquid,  
 $z$  is the height measured upward from the gas outlet,  
 $r$  is the radius,  
 $U$  is the centerline velocity,  
 $b$  is the "plume radius",  
 $\rho_w$  is the mass density of water,  
 $\rho_p$  is the mean mass density of the plume,  
 $S$  is the density effect at the plume centerline,  
 $\lambda$  is the ratio of "gas-containing radius" to "plume radius".

The integral theory to be used follows along lines similar to that in Ref. 1. All the parts of the theory needed for combination with the experimental measurements will be given in the next section.

## 2. THEORY

### 2.1 The Integral Plume Equations

The integral plume theory is based on a principle of local similarity for which radial profiles of velocity have similar forms at different heights as do the radial profiles of density defect. These quantities can then be specified by their centerline values  $U(z)$  and  $S(z)$ ; and their characteristic radii,  $b(z)$  and  $\lambda b(z)$ .

The gas is presumed to follow the isothermal expansion law and mean pressure variations on horizontal planes are presumed to be small enough to have only negligible effects on the plume dynamics. Under these conditions, for a liquid of depth  $H$ , the gas density,  $\rho_g(z)$ , is given by

$$\rho_g(z) = \rho_T (H_B - z) / H_T \quad (2.1)$$

where  $\rho_T$  is the gas density at a pressure of one atmosphere,  $H_T$  is the atmospheric pressure head and  $H_B$  is the pressure head at the level of gas release.

$$H_B = H_T + H \quad (2.2)$$

The integral plume equations will involve the local mean gas fraction,  $f(r, z)$ , which is given by,

$$f(r, z) = \frac{\rho_w - \rho_p(r, z)}{\rho_w - \rho_g(z)} \quad (2.3)$$

and the local gas velocity which will be approximated as the sum of the local liquid speed,  $u(r, z)$  and a constant slip velocity,  $u_b$ , to approximate the effect of the rise velocity of the bubbles relative to the liquid.  $q(z)$ ,  $Q(z)$ ,  $M(z)$  and  $B(z)$ ; the gas volume flux, the liquid volume flux, the momentum flux and the buoyancy per unit height respectively are expressed in terms of local properties as:

$$q(z) = 2\pi \int_0^\infty [u(r, z) + u_b] f(r, z) r dr \quad (2.4)$$

$$Q(z) = 2\pi \int_0^\infty u(r, z) [1 - f(r, z)] r dr \quad (2.5)$$

$$M(z) = 2\pi \int_0^\infty \{u^2(r, z) \rho_w [1 - f(r, z)] + [u(r, z) + u_b]^2 \rho_g(z) f(r, z)\} r dr \quad (2.6)$$

$$B(z) = 2\pi g \int_0^\infty [\rho_w - \rho_g(z)] f(r, z) r dr \quad (2.7)$$

$\gamma$  is called the momentum amplification factor and  $(\gamma-1)/\gamma$  is the fraction of the mean momentum flux that is carried in the turbulence.  $g$  is the acceleration of gravity.

Closure of the integral plume equations requires a relationship between local plume properties and the rate of increase with height of the liquid volume flux. This is provided by the well known entrainment hypothesis which takes the form:

$$\frac{dQ}{dz} = 2\pi\alpha b(z)U(z) \quad (2.8)$$

where  $\alpha$  is the entrainment coefficient. However, whereas all previous investigators considered the entrainment coefficient as a constant to be specified for any particular plume, here it will be considered to be dependent upon local plume properties.

The three integral plume equations can now be determined. The first is the conservation of liquid equation (2.8). The second is the conservation of gas equation which can be expressed as

$$q_{T,H_T}/(H_B-z) = q(z) \quad (2.9)$$

where  $q_{T,H_T}$  is the gas volume flow rate at a pressure of one atmosphere. The third equation results from equating the buoyancy per unit height to the spatial rate of change of momentum flux.

$$B(z) = \frac{dM}{dz} \quad (2.10)$$

## 2.2 Equations for Gaussian Profiles of Velocity and Density Defect

Experimental evidence shows that the radial profiles of velocity and density defect are well approximated by gaussian curves so equations (1.1) and (1.2) will be used henceforth. For these profiles equations (2.4) through (2.7) become:

$$q(z) = \frac{S(z)\pi\lambda^2 b^2(z)}{\rho_w - \rho_g(z)} \left[ \frac{U(z)}{1+\lambda^2} + u_b \right] \quad (2.11)$$

$$Q(z) = \pi U(z) b^2(z) \left\{ 1 - \frac{\lambda^2 S(z)}{[1+\lambda^2][\rho_w - \rho_g(z)]} \right\} \quad (2.12)$$

$$M(z) = \pi b^2(z) \gamma \left\{ U^2(z) \left[ \frac{\rho_w}{2} - \frac{\lambda^2 S(z)}{1+2\lambda^2} \right] + \frac{\lambda^2 u_b \rho_g(z) S(z)}{\rho_w - \rho_g(z)} \left[ \frac{2U(z)}{1+\lambda^2} + u_b \right] \right\} \quad (2.13)$$

$$B(z) = \pi g \lambda^2 S(z) b^2(z) \quad (2.14)$$

The plume equations (2.8), (2.9) and (2.10) then become:

$$2\alpha U(z) b(z) = \frac{d}{dz} U(z) b^2(z) \left\{ 1 - \frac{\lambda^2 S(z)}{[1+\lambda^2][\rho_w + \rho_g(z)]} \right\} \quad (2.15)$$

$$\frac{q_T H_T}{H_B - z} = \frac{\pi \lambda^2 b^2(z) S(z)}{\rho_w - \rho_g(z)} \left[ \frac{U(z)}{1+\lambda^2} + u_b \right] \quad (2.16)$$

$$g \lambda^2 S(z) b^2(z) = \frac{d}{dz} \gamma b^2(z) \left\{ U^2(z) \left[ \frac{\rho_w}{2} - \frac{\lambda^2 S(z)}{1+2\lambda^2} \right] + \frac{\lambda^2 u_b \rho_g(z) S(z)}{\rho_w - \rho_g(z)} \left[ \frac{2U(z)}{1+\lambda^2} + u_b \right] \right\} \quad (2.17)$$

with  $\rho_g(z)$  given by equation (2.1).

### 2.3 Initial Conditions Near the Bottom of the Zone of Established Flow

Equations (2.15), (2.16) and (2.17) can be integrated upward numerically if all parameters are known and if conditions near the bottom of the zone of established flow are known so that the integration can be started. Equation (2.16) for the conservation of gas is valid so two additional conditions are required. The precise determination of these requires unavailable information about the zone of flow establishment, but suitable approximations for most conditions can be made. The reasons for this are that over most of the extent of the plume the momentum gained in the zone of established flow dominates the momentum gained in the zone of flow establishment, and solutions to the plume equations are generally particularly stable to perturbations in initial conditions.

The momentum flux at the height where the integration is to be started,  $z_E$ , is estimated as the sum of the momentum flux coming from the gas outlet and an estimate of the buoyancy in the zone beneath this height. To minimize the error of this estimate,  $z_E$  should be chosen as low as possible so that the buoyancy beneath it is minimized. However, as the height of the gas outlet is approached there is expected to be more error in the first part of the integration due to inaccuracies in both the gaussian approximations and the entrainment hypothesis.

The best choice for  $z_E$  is the one which gives the best balance between these influences. Although this is not known exactly a reasonable position would seem to be the greater of five gas outlet diameters,  $D$ , and the height of the zone of flow establishment for single phase plumes given by Chen and Rodi (1980). This is:

$$z_E = \min \left\{ \begin{array}{l} 5D \\ 10u_o (D/g)^{1/2} [\rho_g(o)/\rho_w]^{3/4} \end{array} \right\} \quad (2.18)$$

where  $u_o$  is the gas velocity at the outlet as determined from the gas volume flow rate and the area of the gas outlet.

Estimating the mean gas speed below  $z = z_E$  as  $u_o/2$ , the estimate for the momentum flux becomes:

$$M(z_E) = q_T \rho_g(H) u_o + \frac{2q(z_E/2)}{u_o} [\rho_w - \rho_g(z_E/2)] g z_e \quad (2.19)$$

Finally, the centerline plume density defect is estimated as:

$$S(z_E) = \rho_w/2 \quad (2.20)$$

It must be emphasized that these cavalier estimates of  $M(z_E)$  and  $S(z_E)$  are not represented as accurate values for the top of the zone of flow establishment, but rather are reasonable values for beginning the numerical integration at  $z = z_E$ . Figure 2.1 is an example of the insensitivity of results over most of the plume of the numerical integration to reasonable variations in the initial conditions.

#### 2.4 Theoretical Framework for Analysis of Velocity Measurements

One use of measurement data is to determine both the entrainment coefficient,  $\alpha$ , and momentum flux amplification factor,  $\gamma$ , at various parts of the plumes. Application of the theory requires a priori specification of the bubble "slip velocity"  $u_b$ , and of the gas/velocity radius ratio,  $\lambda$ .

Photographic measurements of bubble sizes made by the author (for air bubble plumes in water) showed that most of the gas was carried by bubbles whose volumes ranged from 0.01 to 33 cm<sup>3</sup>. Of these, most of the bubbles had volumes between 0.02 and 0.5 cm<sup>3</sup> for which Haberman and Morton (Ref 2) found rise velocities in still water between 0.23 and 0.25 m/s. However, the larger and faster moving

bubbles contain much more volume than the smaller bubbles and Haberman and Morton found a rise velocity of 0.45 m/s for 33 cm<sup>3</sup> bubbles. For the subsequent application of the theory here, a value of 0.35 m/s is used. Figure 2.2 shows an example of the results of numerical integration of the plume equations (2.15), (2.16) and (2.17) for four different values of  $u_b$ ; 0.00, 0.30, 0.35 and 0.40 m/s. The effect of  $\pm 0.05$  m/s variation in  $u_b$  is small, but clearly  $u_b$  cannot be discounted altogether.

By comparing measured gas fraction profiles with measured velocity profiles, Milgram and Van Houten found an average value for  $\lambda$  of 0.8 for their laboratory experiments. No other experimental values are available. However, under the presumption that turbulent velocities scale with mean velocities,  $\lambda$  is expected to be larger (but still less than 1.0) for the larger and faster plumes to be studied here. Figure 2.3 shows an example with values of both 0.8 and 0.9 for  $\gamma$ . The effect of the variation is quite small and a value of 0.8 will be used here in the analysis of the measurements.

The gaussian approximations given by equations (1.1) and (1.2) for radial profiles of velocity and density defect will be used. For each measured radial profile at a height  $z$ ,  $U(z)$  and  $b(z)$  are determined by a fit of equation (1.1) to the data. The local gas density is given by equation (2.1) and the local gas volume flow rate is given by the left hand side of equation (2.16). The local density defect can then be determined from equation (2.11) as,

$$S(z) = \frac{[\rho_w - \rho_g(z)]q(z)}{\pi\lambda^2 b^2(z) [U(z)/(1+\lambda^2) + u_b]} \quad (2.21)$$

The local momentum amplification factor,  $\gamma(z)$  will be obtained as the ratio of the total local momentum flux,  $M_T$ , to the momentum flux of the mean flow,  $M_m$ .

$$\gamma(z) = \frac{M_T(z)}{M_m(z)} \quad (2.22)$$

where  $M_m(z)$  is obtained from equation (2.13) with  $\gamma$  set equal to 1.

The total momentum flux at height  $z$  will be calculated as,

$$M_T(z) = M_T(z_B) + \int_{z_B}^z B(z') dz' \quad (2.23)$$

where the buoyancy per unit height,  $B(z)$ , is given by equation (2.14).

The height  $z_B$  will be taken as the lowest height in the zone of established flow at which conditions are measured or estimated. The momentum flux at  $z_B$  is estimated in the fashion of equation (2.19), but since  $z_B$  is generally considerably greater than  $z_E$  a different estimate for the mean gas speed below  $z_B$  is required. Within a short distance above the height of gas release, the moving material involves a volume flux of water that is of the same order of magnitude as the volume flux of the gas. Therefore the average gas speed below  $z_B$  will be estimated as the average of  $u_o \rho_g(z_B/2)/\rho_w$  and  $[U(z_B) + u_b]$ . Then,

$$M_T(z_B) = q_T \rho_T u_o + 2q(z_B/2) g z_B [\rho_w - \rho_g(z_B/2)] / [u_o \rho_g(z_B/2)/\rho_w + U(z_B) + u_b] \quad (2.24)$$

Because of uncertainty of the buoyancy below  $z_B$ ,  $M_T$  evaluated in this way cannot be expected to be accurate enough for quantitative estimates of  $\gamma$  at  $z_B$ . For all measurement heights above  $z_B$  that are used,  $M_T(z) \gg M_T(z_B)$  so that equation (2.23) is expected to be accurate enough for making quantitative estimates of  $\gamma$  by use of equation (2.22).

The other parameter which depends on local conditions to be determined from the experiments is the entrainment coefficient,  $\alpha$ . Although it could be obtained from experimental determination of the terms in equation (2.8), the differentiation of the liquid volume flux would accentuate experimental errors. To avoid this,  $\alpha$  will be determined by an integration of equation (2.8) between heights at which radial velocity profiles are measured. Call these heights  $z_i$  ( $i=1,2,\dots$ ). Then, under the presumptions that  $\alpha$  varies only slightly between  $z_i$  and  $z_{i+1}$  and that the liquid volume flux,  $Q$ , is well approximated by a linear function in this same height interval, the integral of equation (2.8) is solved for  $\alpha$  as

$$\alpha \left( \frac{z_i + z_{i+1}}{2} \right) = \frac{2}{\pi} \frac{Q(z_{i+1}) - Q(z_i)}{[b(z_i) + b(z_{i+1})][U(z_i) + U(z_{i+1})][z_{i+1} - z_i]} \quad (2.25)$$

where  $Q(z)$  is given by equation (2.12).

### 3. EXPERIMENTS

#### 3.1 Facility and Equipment

The experiments took place in Bugg Spring which is a natural sinkhole spring located at Okahumpka, Florida and which is part of the United States Naval Research Laboratory. Figure 3.1 is a cross-sectional profile of the spring. Both currents and spatial temperature variations in the spring are smaller than can be measured with ordinary instruments. A barge which is tightly moored to anchors on the shore by five cables floats on the surface with one edge of the barge over the deepest part of the spring. An existing gantry was extended to a distance of 4.6 m past this edge. A 2.5 meter tall vertical air entry pipe having a 5 cm inside diameter was secured to a concrete anchor block such that the upper open end of the pipe was 50 m below the surface and vertically under the extended end of the gantry. Air was supplied to the bottom of the pipe through a hose from an airflow meter on the barge which in turn was connected by a hose to a rotary screw air compressor on the shore.

Velocity profiles were measured with the use of a horizontal array of 36 vertical current meters configured as a cross as shown in figure 3.2. Each of the two arms of the cross was 12.9 meters long and the distance between adjacent current meters was 0.75 m. This permitted an accurate estimation of the location of the instantaneous center of the plume from the location on each of the arms on the cross at which the velocity was a maximum.

A system of four support cables was used to adjust the height of the cross and to provide horizontal restraint against turbulence-induced motions of the cross. A taut upper cable attached the upper bridle shown in figure 3.2 to the gantry. A taut lower cable attached to the lower bridle passed through a sheave near the air outlet and then to the barge. Two adjacent ends of the cross rode on vertical cables tensioned to about  $10^4$  newtons which led from the edge of the barge to anchor weights on the bottom.

The current meters were made from the mechanical speed detecting parts of Aanderaa current meters and 36 electronic signal conditioners, each of which contained a low-pass filter with a 10 second time constant. The resulting signals were sampled at a rate of Hz through 36 analog-to-digital channels of a digital computer for 10 minutes for each airflow rate and current meter cross height. Each of the groups of 36 samples was obtained in a time interval of about 0.5 millisecond

so the samples can be considered to be simultaneous. Finally, for each channel each set of ten successive samples was averaged together giving 60 of these short-time averaged measurements for each of the 36 channels in a ten minute measurement period. These measurements were made for airflow rates of 0.024, 0.118, 0.283 and 0.590  $\text{N m}^3/\text{s}$ ; and for heights above the air outlet of 16.47, 25.62, 37.81, 43.90 and 46.95 meters.

### 3.2 Data Reduction

The purpose of the data reduction was to fit a gaussian function as given in equation (1.1) to every radial profile measured with respect to the instantaneous location of the plume centerline and thereby obtain values for the centerline velocity,  $U$ , and the plume radius,  $b$ . This was done by the following steps:

1. For each 36 point, 10 second velocity average, there were 18 values along one axis of the measuring cross and 18 values along the other. Spline cubic interpolating functions were fit to each of these 18 sets of points. The location of the maximum of each of these functions was taken as the value in "cross coordinates" for the location of the plume center. The distance from this location to each of the current meters was determined so that 36 sets of values ( $u,r$ ) were obtained. This was done for all 60 sets of 10 second averages so that 2160 pairs of ( $u,r$ ) values were obtained for each airflow rate and measurement height.
2. The range of values of radius,  $r$ , was partitioned into segments 0.08 meters long. The values of  $u$  for all the  $r$  values falling in any particular segment were averaged together to obtain a value of  $u$  for the midpoint of the segment. This reduced the number of pairs of ( $u,r$ ) values for each airflow rate and measurement height to about 100. Figure 3.3 shows an example of a plot of these values.
3. A gaussian function of the form of equation (1.1) was fit to the reduced data points with  $U$  and  $b$  chosen to minimize the standard deviation between the function and the points. Figure 3.3 shows the gaussian approximation to its data.
4. The above procedure gave 20 radial profiles of velocity. The one for a measurement height of 46.95 m at an airflow rate of 0.118  $\text{N m}^3/\text{s}$  was "out of line" with other profiles and the measured profile had excessive scatter. Therefore this profile was eliminated from the data leaving 19 of these larger scale profiles available for analysis.

5. The current meters measured velocities in the  $(r,z)$  plane. Since the radial mean velocities are small in comparison to the vertical mean velocities, their effects on the measured mean velocities are small. However, a small correction can be, and was, made for this. For each airflow rate the values of  $b(z)$  and  $U(z)$  were fit by spline cubic functions so that their derivatives could be easily evaluated. Then, using the form of equation (1.1) and a radial integration of the continuity equation ( $\text{div } \vec{V}=0$ , neglecting here the effects of the variation in mean density) gave the small radial velocity. From this and the measured velocities in the  $(r,z)$  plane, the vertical velocity components were calculated. These radial profiles of vertical velocity were then fit with gaussian curves as before. The results are shown in table 1.

#### 4. DATA ANALYSIS

##### 4.1 The Data Set

The goals of the data analysis are the determinations of the entrainment coefficient,  $\alpha$ , and the momentum amplification factor,  $\gamma$ . Thus the data to be used here are in the form of values  $b(z)$  and  $U(z)$  at each airflow rate.

The lowest measurement height was 32% of the water depth and this is too high for application of equation (2.24). A low enough point was estimated by an application of the integral theory. This was done as follows. For each airflow rate, the plume equations (2.15), (2.16) and (2.17) were numerically integrated several times starting at a height  $z_E$  as given by equation (2.18); each time with different values of  $\alpha$  and  $\gamma$  which were taken, for this step only, to be independent of height. The integration which best fit the measured values of  $b(z)$  and  $U(z)$  was chosen in each case. An example of this is shown in figure 4.1. As is demonstrated in figure 2.1, errors in initial conditions for beginning the integration are most influential in the region below the minimum (maximum negative) slope of the function  $U(z)$ . Therefore, a value of  $z_B$  was chosen for application of equation (2.24) that was above this point of minimum slope and the required values of  $U(z_B)$  and  $b(z_B)$  were obtained from the numerical integration. The value used for  $z_B$  was 1.98 m.

Values of  $b(z)$  and  $U(z)$  were fit with spline cubic functions. Instead of forcing these functions to fit all the data points exactly, functions with four equally spaced nodal points with extrapolated end point curvatures were used subject to the criterion of minimum variance with the unsmoothed data. Since data at five or six heights were used, this process introduced a small amount of data smoothing. The spline cubic functions were used for the remainder of the data analysis. Table 1 shows both the unsmoothed data and the evaluations of the spline cubic functions. At each data height these evaluations were used together with equations (2.21) and (2.14) to determine the centerline density defect and the buoyancy per unit height which was then in turn fit with a four nodal point cubic spline function. This was then integrated by quadrature to evaluate equation (2.23) at each data height. With this done, the momentum amplification factor was evaluated from equation (2.22) at each data height except for the  $z_B$ 's and these values are also shown in table 1. Finally, table 1 shows the values of the liquid volume flux,  $Q(z)$  which were determined from equation (2.12).

The values of the entrainment coefficient,  $\alpha$ , were determined from equation (2.25) at positions midway between data heights and these are shown in table 2.

## 5. CONCLUSIONS

The integral plume theory, which has been used successfully in the past to describe plumes of laboratory scale, has been found to be applicable to plumes of larger scale as well. The entrainment coefficient has been found to increase with increasing gas flow rate for the large scale plumes and this is consistent with the same finding at laboratory scale. The entrainment coefficient, itself being dimensionless, must depend on dimensionless plume parameters which must include the gas flow rate in their formulation. Details of the relationship between the entrainment coefficient and the dimensionless plume parameters will be published in the future.

For the small scale laboratory plumes described in ref. 1 the mean momentum flux carried by the turbulence was of the same order of magnitude as the mean momentum flux carried by the mean flow. For the larger scale plumes described here only a small fraction of the mean momentum flux was carried by the turbulence. Thus we can conclude that the fraction of the mean momentum flux carried by the turbulence also depends on the dimensionless plume parameters. Details of the dependency will be published in the future. However, here we can conclude that for plumes having the scale of a subsea hydrocarbon well blowout, nearly all of the mean momentum flux is carried by the mean flow.

## ACKNOWLEDGEMENTS

This work was supported in part by the U.S. Department of the Interior under contract number 14-08-001-20460, and in part by the Office of Naval Research under contract number N00014-81-K-0785.

REFERENCES

1. MILGRAM, J.H. & VAN HOUTEN, R.J. "Plumes From Sub-Sea Well Blowouts".  
Proc. of the Third Int'l Conf., BOSS. 1, 659-684, 1982.
  
2. HABERMAN, W.L. & MORTON, R.K. "An Experimental Study of Bubbles Moving  
in Liquids". Proc. of the Amer. Soc. of Civil Eng. 80, Separate #387, 1954.

Z	RAW		SMOOTH		q	B	S	GAMMA	N M <sup>3</sup> /S AIRFLOW
	b	U	b	U					
1.98	0.162	1.129	0.150	1.127	0.0042	0.077	88.21		
16.47	1.540	0.489	1.572	0.506	0.0055	3.929	1.68	1.24	
25.62	1.920	0.515	1.967	0.477	0.0070	5.797	1.40	1.50	
37.81	2.822	0.498	2.466	0.562	0.0109	10.725	1.28	1.16	0.024
43.90	2.470	0.608	2.895	0.553	0.0149	14.555	1.29	1.15	
46.95	2.980	0.538	3.191	0.519	0.0184	16.503	1.25	1.26	
1.98	0.298	1.543	0.257	1.542	0.0204	0.306	118.20		
16.47	1.780	0.860	1.732	0.866	0.0272	8.124	5.12	1.23	
25.62	2.380	0.829	2.476	0.823	0.0345	15.834	3.27	1.14	0.118
37.81	3.333	0.833	3.621	0.888	0.0534	34.475	2.24	0.91	
43.90	4.455	0.745	4.684	0.743	0.0735	44.811	2.36	1.07	
1.98	0.333	1.739	0.328	1.740	0.0490	0.552	159.24		
16.47	2.330	1.114	2.359	1.109	0.0653	19.351	5.95	0.95	
25.62	3.590	0.970	3.583	0.971	0.0827	39.102	3.99	0.83	
37.81	5.568	0.981	5.385	0.906	0.1280	81.840	2.44	0.77	0.283
43.90	5.976	0.912	6.393	0.861	0.1762	110.426	2.45	0.81	
46.95	7.190	0.794	6.955	0.823	0.2172	124.919	2.62	0.88	
1.98	0.395	2.103	0.412	2.105	0.1022	1.041	182.09		
16.47	2.609	1.326	2.488	1.316	0.1362	25.493	9.44	0.99	
25.62	3.399	1.174	3.615	1.188	0.1723	48.652	6.08	0.99	
37.81	5.556	1.189	5.296	1.184	0.2668	104.145	4.40	0.83	0.590
43.90	6.108	1.171	6.343	1.162	0.3674	146.677	4.28	0.81	
46.95	7.030	1.121	6.944	1.129	0.4527	170.688	4.49	0.84	

TABLE 1. The Momentum Amplification Factors and Plume Properties Obtained from the Data Analysis at the Measurement Heights

Z	b	U	q	S	ALPHA	N M <sup>3</sup> /S AIRFLOW
9.23	0.86	0.817	0.0047	44.95	0.060	
21.05	1.77	0.492	0.0062	1.54	0.037	
31.71	2.22	0.520	0.0085	1.34	0.056	0.024
40.86	2.68	0.557	0.0126	1.28	0.067	
45.43	3.04	0.535	0.0165	1.32	0.063	
9.23	0.99	1.203	0.0234	61.66	0.072	
21.05	2.10	0.843	0.0304	4.16	0.076	0.118
31.71	3.05	0.831	0.0419	2.81	0.096	
40.86	4.00	0.780	0.0618	2.35	0.085	
9.23	1.34	1.425	0.0560	82.43	0.108	
21.05	2.97	1.040	0.0730	4.52	0.111	
31.71	4.47	0.938	0.1004	2.91	0.133	0.283
40.86	5.88	0.883	0.1483	2.44	0.144	
45.43	6.67	0.842	0.1946	2.53	0.135	
9.23	1.45	1.710	0.1168	95.77	0.108	
21.05	3.05	1.252	0.1521	7.76	0.106	
31.71	4.46	1.186	0.2094	5.24	0.137	0.590
40.86	5.82	1.173	0.3091	4.34	0.163	
45.43	6.64	1.146	0.4056	4.39	0.165	

TABLE 2. The Entrainment Coefficients and Plume Properties at Heights Midway Between Measurement Heights

The entrainment coefficients have been evaluated by equation (2.25) and the properties b, U, q and S are the averages of the values above and below the midpoints.

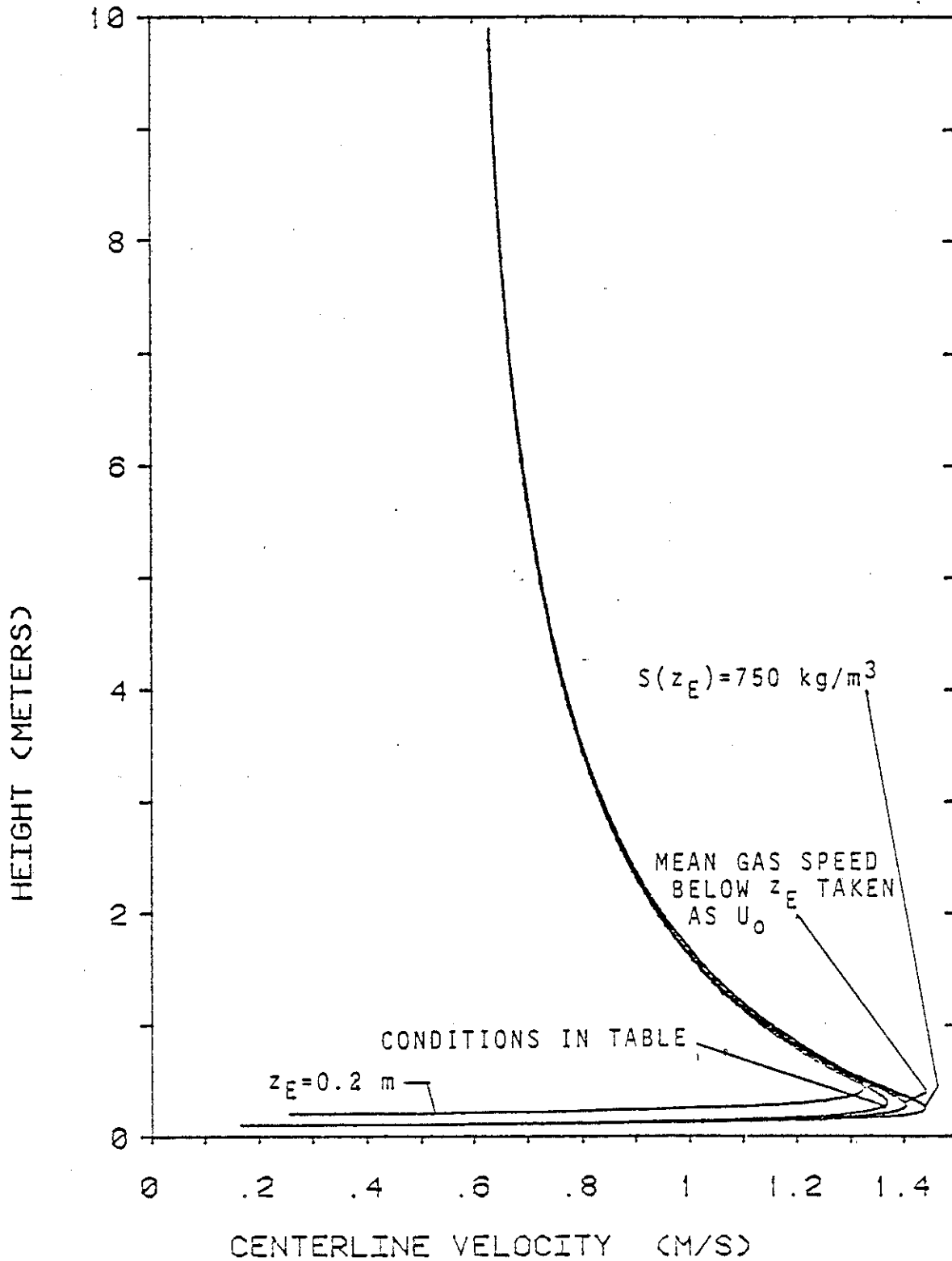


FIGURE 2.1 The Effect of Variations in Initial Conditions for Starting the Numerical Integrations

Conditions are as listed below except for notations on individual curves.

$H = 10 \text{ m}$	$Z_E = 0.1 \text{ m}$	$g = 9.81 \text{ m}^2/\text{s}$	$q = 0.01 \text{ N m}^3/\text{s}$	$S(z_E) = 500 \text{ Kg/m}^3$
$u_0 = 25 \text{ m/s}$	$\rho_T = 1.3 \text{ Kg/m}^3$	$\rho_w = 1000 \text{ kg/m}^3$	$\lambda = 0.8$	$\gamma = 1.5$
$u_b = 0.35 \text{ m/s}$	Mean gas speed below $Z_E$ taken as $u_0/2$			

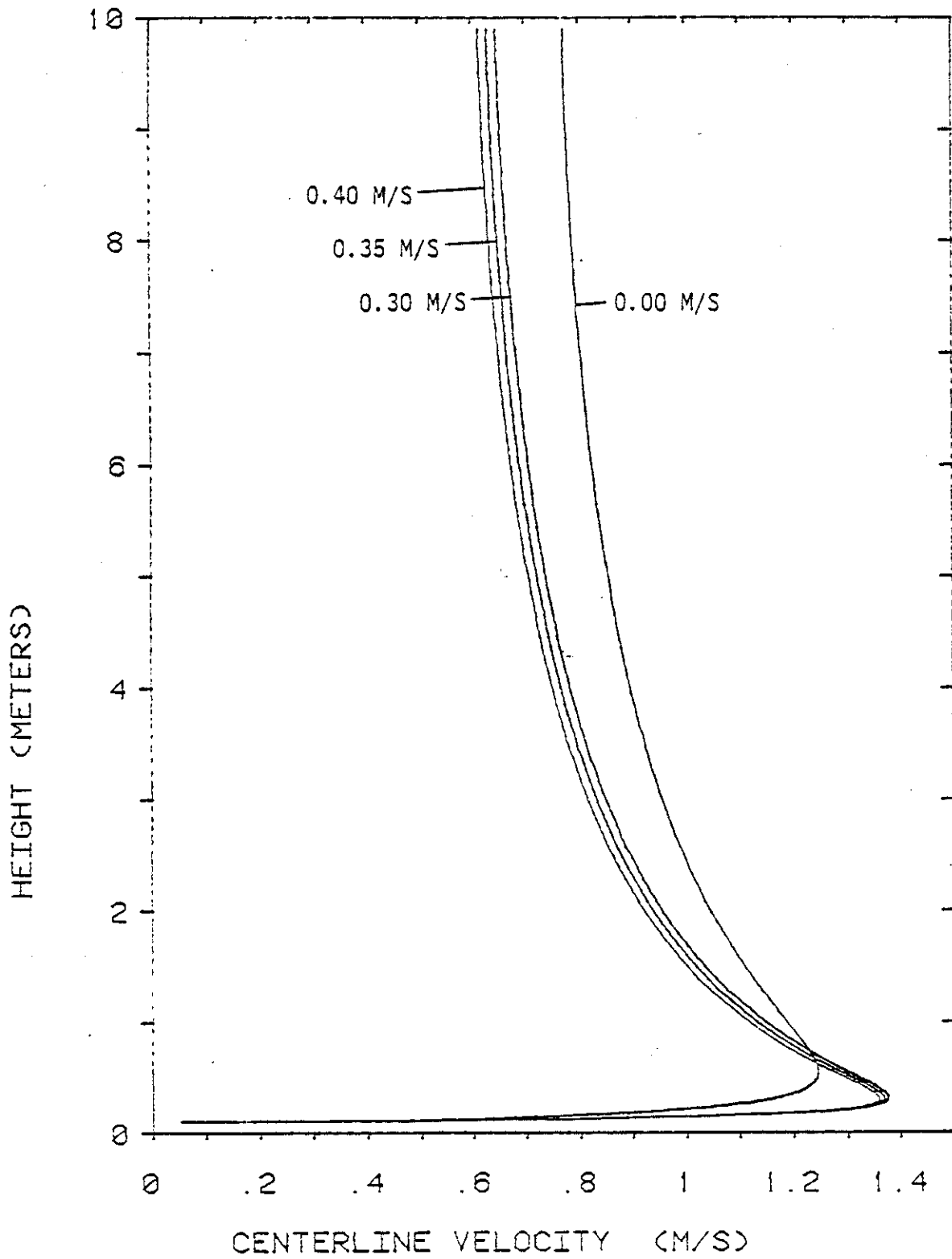


FIGURE 2.2 Effect of Gas Bubble Slip Speed on Solution to the Plume Equations  
The bubble slip speeds used in the calculations are shown on each curve.  
Other conditions are as given in figure 2.1.

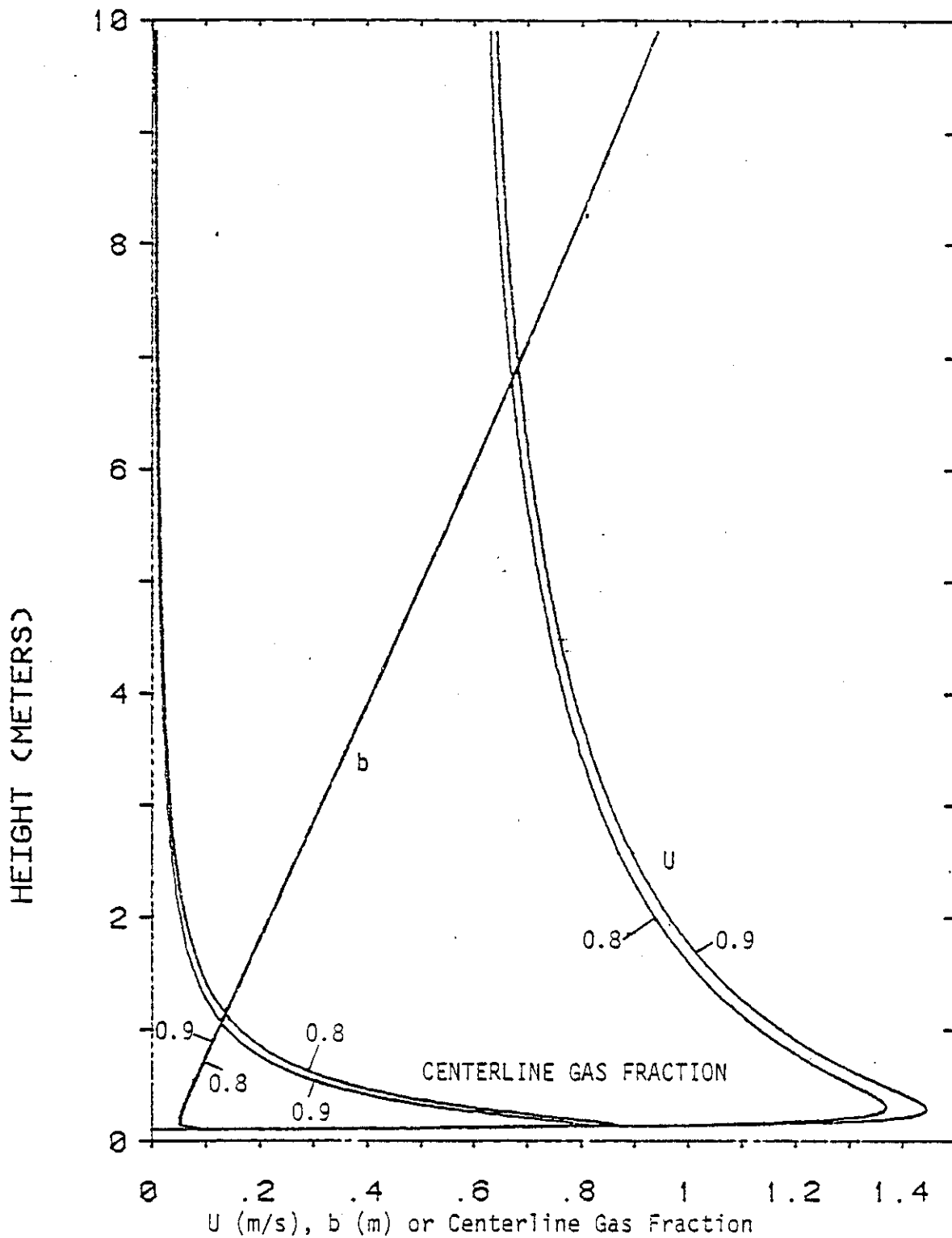


FIGURE 2.3 Numerical Results for Gas-Velocity Radius Ratios,  $\lambda$ , of 0.8 and 0.9. The conditions for the calculations are those given in figure 2.1. The values for  $\lambda$  are shown on the curves. The difference in plume radius,  $b$ , for the two values of  $\lambda$  is almost undiscernable.

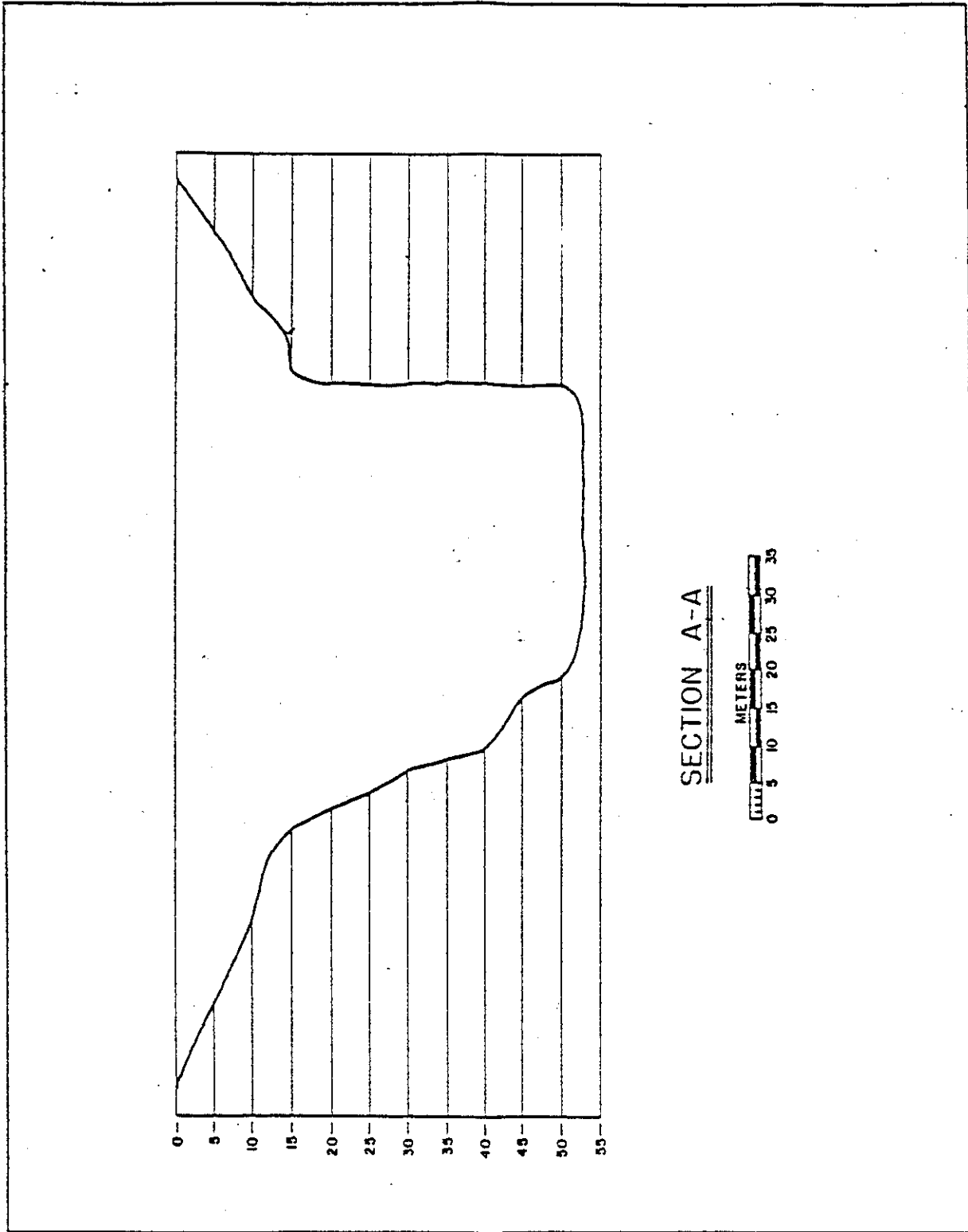


FIGURE 3.1 A Depth Profile of Bugg Spring

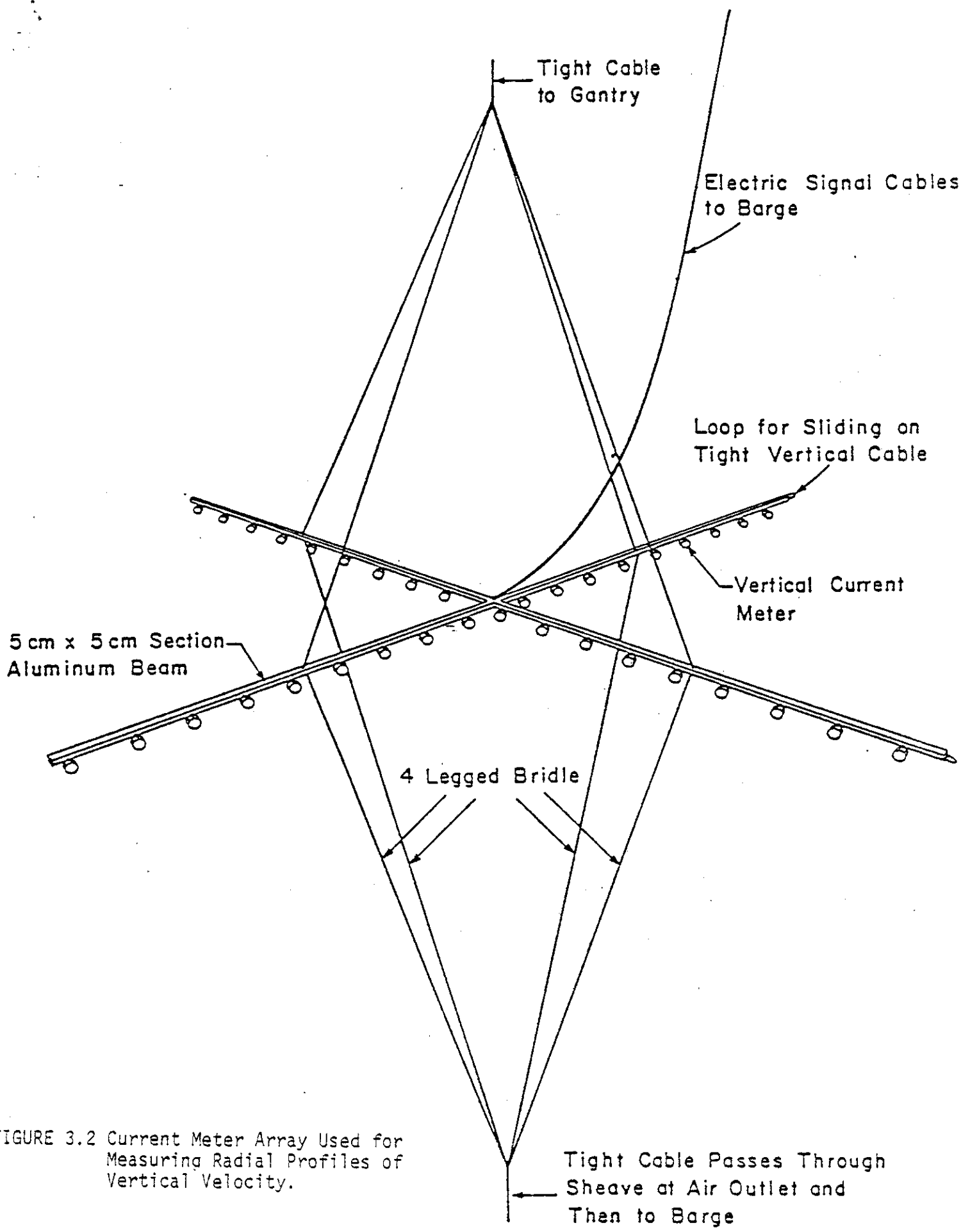
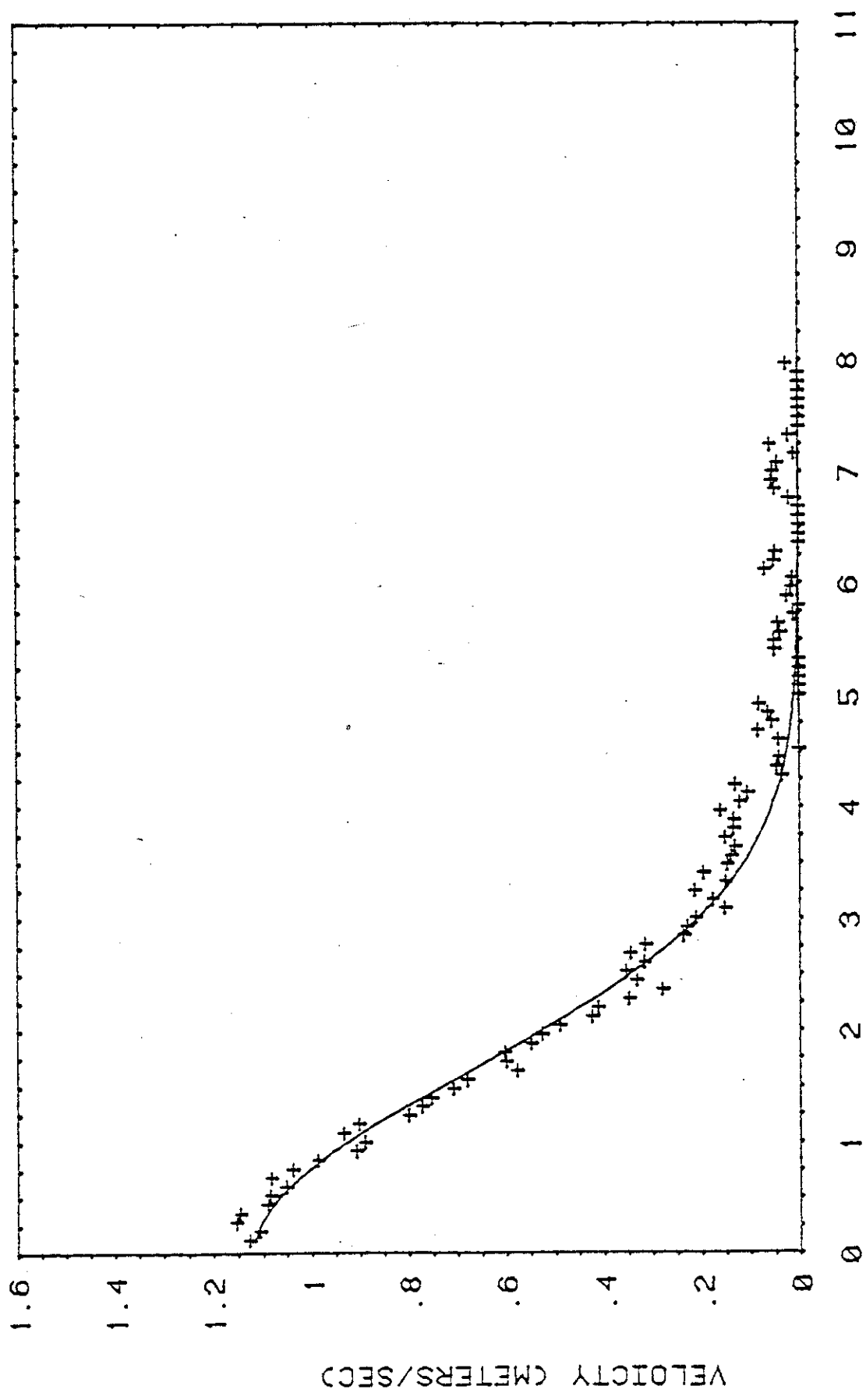


FIGURE 3.2 Current Meter Array Used for Measuring Radial Profiles of Vertical Velocity.



RADIUS (METERS)

FIGURE 3.3 An Example of Reduced Data for a Radial Profile of Vertical Velocity  
The case shown is for a gas flow rate of  $0.283 \text{ N m}^3/\text{s}$  and a height of 16.47 m above the gas outlet.  
+ reduced data point      \_\_\_\_\_ Gaussian function fit to the data

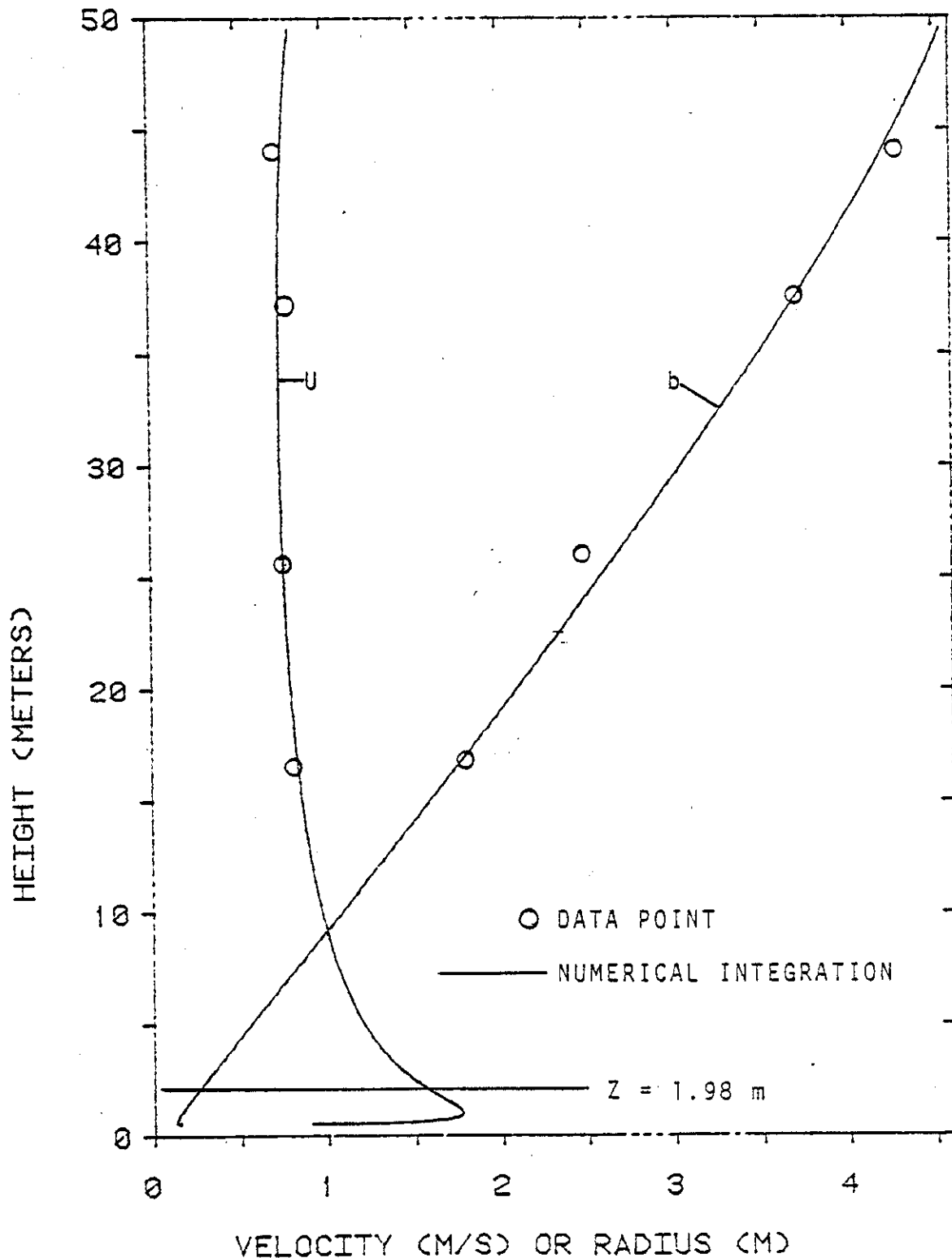


FIGURE 4.1 Example of a Numerical Integration Used to Estimate Conditions at a Low Point in the Zone of Established Flow

The conditions of the example correspond to an airflow rate of  $0.118 \text{ N m}^3/\text{s}$  in the Bugg Spring Experiments. The numerical integration was done with  $\lambda=0.8$ ,  $Z_E=0.5 \text{ m}$  and  $S(z_E)=500 \text{ kg/m}^3$ . The best fit to the data was with  $\gamma=1.1$  and  $\alpha=0.087$  which is the case that is shown.